# Vascular resistance arm of the baroreflex: methodology and comparison with the cardiac chronotropic arm

Krohova, J.[1], Faes, L.[2], Czippelova, B.[1], Pernice, R.[2], Turianikova, Z.[1], Wiszt, R.[1], Mazgutova, N. [1], Busacca, A. [2], Javorka, M. [1]

[1]Department of Physiology and Biomedical Centre Martin (BioMed Martin), Jessenius Faculty of Medicine, Comenius University, Martin, Slovakia

[2]Department of Engineering, University of Palermo, Italy

Running head: High-pressure baroreflex: vascular resistance arm analysis

Corresponding author:

Prof Michal Javorka, MD PhD
Department of Physiology
Jessenius Faculty of Medicine in Martin
Comenius University in Bratislava
Mala Hora 4C, 03601 Martin, Slovakia
E-mail: michal.javorka@jfmed.uniba.sk

## Abstract

Baroreflex response consists of cardiac chronotropic (effect on heart rate), cardiac inotropic (on contractility), venous (on venous return) and vascular (on vascular resistance) arms. Because of its measurement simplicity, cardiac chronotropic arm is most often analysed. The aim was to introduce a method to assess vascular baroreflex arm, and to characterize its changes during stress. We evaluated the effect of orthostasis and mental arithmetics (MA) in 39 (22 female, median age: 18.7 yrs.) and 36 (21 female, 19.2 yrs.) healthy volunteers, respectively. We recorded systolic and mean blood pressure (SBP and MBP) by volume-clamp method and R-R interval (RR) by ECG. Cardiac output (CO) was recorded using impedance cardiography. From MBP and CO, peripheral vascular resistance (PVR) was calculated. The directional spectral coupling and gain of cardiac chronotropic (SBP to RR) and vascular arms (SBP to PVR) were quantified. The strength of the causal coupling from SBP to PVR was significantly higher than SBP to RR coupling during whole protocol ($P < 0.001$). Along both arms, the coupling was higher during orthostasis compared to supine ($P < 0.001$ and $P = 0.006$), no MA effect was observed. No significant changes in the spectral gain (ratio of RR or PVR change to a unit SBP change) across all phases were found ($0.111 \leq P \leq 0.907$). We conclude that changes in PVR are tightly coupled with SBP oscillations via the baroreflex providing an approach for the baroreflex vascular arm analysis with a potential to reveal new aspects of blood pressure dysregulation.



Keywords: arterial baroreflex; vascular resistance; impedance cardiography; spectral coupling


## New & Noteworthy

Baroreflex response consists of several arms but cardiac chronotropic arm (blood pressure changes evoking heart rate response) is usually analyzed. This study introduces a method to assess vascular baroreflex arm from the continuous noninvasive measurement of

peripheral vascular resistance as an output considering causality in the interaction between oscillations and slower dynamics of vascular tone changes. We conclude that while vascular baroreflex arm involvement become dominant during orthostasis, gain this interaction is relatively stable.

## Introduction

The high-pressure baroreflex (BR) has a principal role in the short-term regulation of arterial blood pressure and blood flow (22). The output of brainstem centers is sent to effectors by efferent pathways influencing various cardiovascular parameters. As a response to blood pressure changes, four major cardiovascular control targets are influenced via high-pressure baroreflex, *i.e.* heart rate, cardiac contractility, peripheral vascular resistance (PVR) and venous tone (Fig. 1), aiming on the main objective to buffer variations in arterial blood pressure (24, 32, 33). In detail, a decrease in arterial blood pressure evokes a baroreflex response including an increased heart rate (cardiac chronotropic BR arm) and vasoconstriction mostly occurring in the arterioles (vascular resistance BR arm). Conversely, an increase in arterial blood pressure is accompanied by opposite effects (55, 57).

Cardiovascular diseases are often accompanied by an impairment of BR control associated with imbalance in the autonomic outflow often resulting in a chronic sympathetic overactivity (23). Moreover, in healthy subjects BR control mechanisms act in response to physiological stressors such as change of posture, mental workload and others (10, 29, 52). Therefore, evaluation of the baroreflex function can provide valuable information for the assessment of cardiovascular regulation in normal and pathological conditions. Although all the various components of BR have the same main objective to buffer variations in arterial blood pressure, they are not fully redundant and it is assumed that they operate at least partially independently (12, 53). The cardiac chronotropic BR arm is the most frequently

studied BR component due to the simplicity of obtaining non-invasive measurements of heart rate variations from the ECG (7, 42).

While the other BR arms were studied only rarely so far (53, 57, 68), a simultaneous assessment of the various components could give a more complete picture of the baroreflex regulation (7, 11, 53, 55). Another important aspect often overlooked in previous studies is that the evaluation of the cardiac arm and other arms of the baroreflex must take into account: (i) the oscillatory nature of cardiovascular parameters, being able to separate contributions occurring in different frequency bands (typically divided in very low frequency (VLF, up to 0.04 Hz), low frequency (LF, 0.04 – 0.15 Hz), and high frequency (HF, 0.15 – 0.4 Hz) bands) (8); and (ii) the closed-loop nature of cardiovascular interactions and the effects of exogenous variables like respiration, which demand to adopt causal approaches to perform a proper evaluation (15, 54).

Although several previous studies were also focused on the vascular baroreflex arm analysis they contained some important methodological limitations mostly related to the selection of output signal. Often the PVR as an output signal was substituted by surrogate signals including muscle sympathetic nerve activity (62, 64), pulse transit time (63) or diastolic blood pressure employing various modelling strategies to assess relationship of output signal to input blood pressure oscillations (1, 6). To the best of our knowledge, this is the first study considering three important aspects of vascular baroreflex analysis: selection of PVR as a target signal, considering the causality between blood pressure changes and PVR, and focusing on slower oscillations only.

The main aim of this study is to introduce a comprehensive methodology for the noninvasive assessment of the vascular resistance arm of the baroreflex from spontaneous PVR and arterial pressure oscillations. To this end, we combine the volume-clamp photoplethysmography and impedance cardiography techniques to measure systolic blood

pressure (SBP) and PVR, and to assess the directional interactions from SBP to PVR through a causal spectral decomposition technique which allows to separate causal from non-causal contributions while focusing on LF oscillations in the computation of coupling and gain measures. Employing this approach, the behavior of the vascular resistance arm of the baroreflex is investigated together with that of the cardiac chronotropic arm in a group of healthy subjects monitored under different physiological conditions including orthostatic test and mental challenge, also studying gender differences.

## Methods

The effect of orthostasis was evaluated in a group of 39 healthy volunteers (22 female, median age: 18.7 yrs.), while the effect of mental arithmetic task was evaluated in a group of 36 healthy volunteers (21 female, median age: 19.2 yrs.). Participants were instructed not to use substances influencing autonomic nervous system or cardiovascular system activity during 24 hours before the measurement. Female subjects were examined in the proliferative phase ($6^{th}$ – $13^{th}$ day) of their menstrual cycle. The experimental protocol is described in more details elsewhere (31). Briefly, four experimental conditions were considered in this study: supine rest (15 min); head-up tilt (HUT, the subject was tilted to 45 degrees on the motor driven tilt table for 8 min to evoke mild orthostatic stress); supine recovery in the resting supine position (10 min); and non-verbal mental arithmetic task (MA) in the supine position (6 min). There were no signs of presyncope in any subject during the orthostatic challenge. The subjects breathed spontaneously without any effort to control breathing rate or tidal volume. The frequency of breathing in all subjects was in the range of high frequency oscillations (minimal breathing rates during all four phases of examination protocol were 0.25 Hz). The study was approved by Ethical Committee of the Jessenius Faculty of Medicine, Comenius University and all participants signed a written informed consent.

*Data Acquisition and Analysis*

We recorded non-invasively beat-to-beat values of R-R interval (RR) by ECG (CardioFax ECG-9620, NihonKohden, Japan), and of systolic and mean blood pressure (SBP and MBP, respectively) by the photoplethysmographic volume-clamp method (Finometer Pro, FMS, Netherlands). MBP was calculated as the true integrated mean pressure between the current and the next pressure upstroke. Cardiac output (CO) was recorded using impedance cardiography (CardioScreen® 2000, Medis, Germany). Then, PVR was calculated for each heart beat as the ratio of MBP and CO (PVR = MBP / CO), assuming zero venous pressure at the right atrium (37, 67).

To avoid transient changes, the following segments of 300 beats were extracted from the original recordings for data analysis as follows: during supine rest the segment started 8 min after the beginning of the supine rest phase; during HUT the segment started 3 min after the change of the position; during supine recovery the segment started 7 min before starting the MA task; and during MA the segment started 2 min after the beginning of the last phase.

In some cases, due to the presence of noise and artefacts, the impedance cardiograph was not able to detect important reference points on the recorded impedance cardiogram waveform and thus to calculate the hemodynamic parameters (CO) on the beat-to-beat basis. If the number of missing values in the 300 heart beats long time series did not exceed 15 and no more than 4 were found in a row, cubic spline interpolation was applied to substitute missing values. Otherwise, the recording was excluded from the analysis.

All signals were detrended to avoid the effect of long-term trends on the data analysis employing zero phase IIR high-pass filter with a cut-off frequency at -3dB equal to 0.0107 cycles/beat (48). The analysis of cardiac chronotropic and vascular resistance arms of BR was carried out in the frequency domain, computing measures of spectral causality

(a measure of the causal coupling strength between two signals, here directed along the baroreflex (interactions from SBP to RR interval and from SBP to PVR, respectively)) and spectral gain (a measure of the target response magnitude (RR or PVR change) corresponding to a unit change in SBP; *i.e.* baroreflex sensitivity). These measures were derived from a recently proposed partial spectral decomposition method based on the linear parametric representation of multivariate autoregressive processes (14). This method is a modification of the causal coherence (54), a measure that quantifies in the frequency domain the very popular concept of Granger causality defined for linear bivariate parametric models (21). The modification allows, thanks to the use of spectral decomposition (6), to associate Granger causality to specific oscillatory components commonly found in the two observed signals. The method is described with mathematical details in the Appendix. It allows to separate a power spectral density function into spectral components which are related to specific oscillations having their associated central frequency and power; the components are identified automatically from the oscillatory content specific to each analyzed pair of signals. Then, from each oscillatory component of the target signal (here, RR or PVR), the contribution of the driver signal (here, SBP) to this component is estimated and used in the computation of the causal measures of coupling and gain. Importantly, here we focused the analysis on low frequency oscillations only (LF, 0.04 to 0.15 Hz) in order to minimize the effect of non-baroreflex mechanisms on the assessed measures. The method for causal spectral decomposition is described in Fig. 2 for the time series of SBP, RR and PVR measured from a representative subject in the resting supine position.

*Statistical analysis*

Due to the observed non-gaussian distribution of the measures assessed across subjects, nonparametric tests were used for statistical analysis. The statistical comparison between the spectral causality/gain computed along the direction from SBP to RR (cardiac

chronotropic arm of BR) and the direction from SBP to PVR (vascular resistance BR arm) and between two subsequent phases (supine rest *vs.* HUT, or supine recovery *vs.* MA) was performed by the Wilcoxon signed-rank test. Differences between gender groups were evaluated by Mann-Whitney U test. All results were considered statistically significant at a P value $< 0.05$. The statistical analysis was performed using SYSTAT 13 (Systat Software Inc., USA). The effect sizes were quantified by: Kendall's W (comparison of supine rest vs. HUT, or supine recovery vs. MA) and by dividing the absolute (positive) standardized test statistic Z by the square root of the number of pairs ($n = 39$ or $n = 36$) (between group difference). According to Cohen's classification of effect sizes, the values 0.1, 0.3 and 0.5 indicating small, medium and large effects, respectively.

**Results**

Table 1 represents the group average ($n = 39$ for supine rest and HUT phases and $n = 36$ for supine recovery and MA phases) of the mean and SD of the beat to beat RR, SBP, MBP, DBP, CO, PVR and breathing frequency data during resting phases and two stress conditions (HUT and MA).

Fig. 3 reports the results of the spectral coupling analysis of the cardiac chronotropic BR arm (from SBP to RR) and of the vascular resistance BR arm (from SBP to PVR). The spectral coupling from SBP to PVR was significantly higher than the coupling from SBP to RR during the whole study protocol ($P < 0.001$). The effect size for this comparison was largest during supine rest (Kendall`s $W = 0.780$), while the other effect sizes varied between 0.522 and 0.694. The spectral coupling in both BR arms was significantly higher during HUT compared to the preceding supine rest phase ($P < 0.001$ and $P = 0.007$, respectively). Although both differences were highly statistically significant, the effect of orthostasis on the coupling from SBP to RR was large (Kendall`s $W = 0.632$) whereas the effect of HUT on the coupling from SBP to PVR was only of small size (Kendall`s $W = 0.109$). No significant

differences ($P \geq 0.432$) and small effect sizes only (Kendall`s $W = 0.029 – 0.049$) were found for the variations of the spectral coupling index assessed during MA in comparison with the preceding supine recovery; the result holds for both BR arms ($P \geq 0.432$). No significant gender differences in spectral coupling were found in any of the analyzed phases ($0.347 \geq P \leq 1.000$, effect sizes 0.003 – 0.151).

Fig. 4 reports the distribution of the spectral gain index computed for the cardiac chronotropic (upper row) and the vascular resistance (bottom row) arms of the baroreflex in the supine rest and HUT conditions (left column), and in the supine recovery and MA conditions (right column). No significant changes in spectral gain from SBP to RR or from SBP to PVR were observed across all phases ($0.109 \leq P \leq 0.900$; effect size Kendall`s $W = 0.003 – 0.080$).

As reported in Fig. 5, significant gender differences were observed in the values of spectral gain from SBP to RR computed during the supine rest condition ($P = 0.036$, effect size = 0.336); specifically, the spectral gain was significantly higher in men than in women. Moreover, the spectral gain from SBP to PVR was significantly higher in women during supine recovery and MA phases ($P \leq 0.002$, effect size = 0.492 – 0.522).

## Discussion

The baroreflex is a key component of the cardiovascular autonomic control. The research attention devoted to the baroreflex function by physiologists and clinicians was focused almost exclusively to the assessment of the cardiac chronotropic BR arm. However, it is known that, to achieve a more complete picture about baroreflex regulation, more BR arms should be evaluated simultaneously (7, 11, 53, 55).

### *Physiological aspects*

From the physiological point of view, our study was focused on a comparison between the strength of cardiac chronotropic and vascular resistance arms of baroreflex and on the assessment of the spectral causality and gain behavior during changing physiological states (rest, orthostasis, cognitive load) and on the detection of potential gender differences.

The comparison between the spectral causality measures along the directions SBP→PVR *vs.* SBP→RR performed in the low frequency band showed that PVR changes are more baroreflex-mediated compared to RR interval changes; this was expressed in terms of significantly higher spectral causality values. This indicates that, while PVR is dominantly under BR influence, RR interval variability is also influenced by other (*i.e.* non-baroreflex) mechanisms, mostly at rest and during MA. In general, mechanisms operating along the causal direction opposite to that under investigation (in our case, mechanisms with arterial blood pressure as the target variable) are typically observed in closed-loop physiological control systems. Previous studies documented the importance of the heart period and of the peripheral resistance on arterial pressure oscillations in the LF band, reflecting respectively the cardiovascular feed-forward (direction RR→SBP (17, 30, 31)) and the role of PVR as a source of MAP changes (direction PVR→MAP (3, 13)); it was also shown that CO is not a significant source of arterial blood pressure fluctuations, while it may be only responsible of dampening them through the baroreflex (3). An involvement of the vascular arm of high-pressure baroreflex as an important source of PVR variability was also demonstrated in previous studies in dogs (46) and humans (5, 25).

We have evaluated the changes in the characteristics of the vascular resistance and cardiac chronotropic BR arms during passive orthostasis (HUT) and cognitive load (MA). We have chosen HUT and MA as the tests frequently used in the autonomic nervous system control testing. During HUT, the impact of gravity causes venous pooling of the blood in the lower part of the body and a consequent decrease of arterial blood pressure is sensed by

baroreceptors. As a response mostly involving baroreflex, parasympathetic inhibition and sympathetic activation leads to heart rate and peripheral vascular resistance increase (10, 19). In contrast, while the MA task is accompanied by similar responses, central mechanisms independent of the baroreflex are responsible for them (38, 66). According to an expected involvement of the baroreflex in reactions related to orthostasis, we observed a significant increase in the spectral coupling in both BR arms during HUT underlining their importance during orthostatic challenge. On the other hand, no significant change in spectral coupling in any BR arm was associated with MA.

Our findings confirm the well-known stronger involvement of cardiac chronotropic BR during orthostatic challenge represented by the higher values of the causal coupling from SBP to RR (16, 17, 28, 30, 42, 49). In contrast, the observations on vascular baroreflex arm involvement changes during orthostatic test were only scarcely reported. Contrary to our observations, a tendency to a decreased contribution of systolic blood pressure to diastolic blood pressure oscillations – a surrogate measure of vascular baroreflex arm involvement used in several previous studies – was observed during lower-body negative pressure (a test simulating blood shift in orthostatic test) (2). Interestingly, this study demonstrated an increased vascular arm involvement after prolonged (2 months) head-down bed rest simulating microgravity conditions. Applying the same approach, the changes in vascular baroreflex arm involvement during exercise with different intensities were inconsistent (1). The causal analysis (using modified sequence method) of both BR arms during HUT was used in study by Marchi et al. (42), where the invasively measured MSNA was used for evaluation of the vascular resistance BR arm. They found an increased involvement of both arms during graded HUT ranging from 0 to 60 degrees. Our results confirm these findings of the stronger BR involvement in both analyzed arms using a novel methodology considering important physiological features of the BR function.

Focusing on the response to MA, the simultaneous non-invasive evaluation of both BR arms was previously performed using the non-casual sequence method in young healthy volunteers, where decreased baroreflex effectiveness as an index derived from sequence method (a measure of coupling strength) of both arms was found in the sedentary group but not in the active one (57). It should be stressed that although the previous studies achieved important results in the field of vascular baroreflex arm analysis their results are not directly comparable to our results due to a different methodology applied in them. The evaluation of coupling between parameters characterizing the vascular resistance BR arm was mainly performed employing the non-causal approaches using the MSNA (20, 35, 51) as an output signal.

We did not find any significant difference in SBP→RR and SBP→PVR spectral gain across all phases. This suggests that the gain of the reflexes remains relatively stable in spite of the significant changes in the spectral coupling documented during the various challenges. Although many previous studies employing non-causal methods demonstrated a decrease in gain in SBP – RR relationship during stress conditions (10, 35, 50, 51, 59), such decrease could be attributed to the decreased feedforward connection between RR and SBP (29, 42). Our results are based on causal methods enabling to assess BR related interactions in more clear way. Similar results were found in previous studies, which have applied the causal approaches in frequency domain (LF band) for evaluation of cardiac chronotropic BR sensitivity during HUT (15, 41) and MA task (28).

Several studies indicated less-responsive cardiovascular functions in women compared to men (9, 12). While the spectral coupling strength in both arms was similar, we have found some gender differences in spectral gains. Our results indicate that while unit blood pressure change at rest evokes bigger response in heart rate in males, the response in PVR is more

prominent in females. This is a novel finding requiring more refined study on the involvement of different BR arms in relation to gender.

*Methodological aspects*

Our study was focused on introducing a noninvasive method for the quantitative assessment of the vascular resistance arm of the baroreflex. From a methodological point of view, the analysis of other BR arms, including the vascular resistance arm, should take into consideration several important issues. Firstly, for the analysis of the vascular resistance BR arm, the target signal should be selected. The majority of previous studies in this field used invasive recordings of the sympathetic activity directed to vessels in the lower extremities of the body, e.g. using the microneurographic recording of muscle sympathetic nerve activity (MSNA) from the peroneal nerve (4, 62, 64). This method has several disadvantages, including its invasiveness and the difficulty of finding and maintaining of the correct recording position for electrode, which makes the signal noisy and its amplitude unstable and unreliable (39, 42). In addition, although the overall vascular resistance (PVR) is a target parameter of this BR arm, the recording comes from a limited part of the circulation.

In our study we used impedance cardiography (in connection with volume-clamp photoplethysmographic blood pressure measurement) to assess PVR. This brings the advantage of being able to measure the stroke volume measurement directly from the oscillations in thoracic impedance, with no necessity of estimating the vascular characteristics; on the contrary, using the pulse contour method the vascular physical characteristics need to be estimated from anthropometric data (26, 65).

Secondly, although basic cardiovascular parameters such as the heart rate, the systolic blood pressure and others, oscillate spontaneously from beat to beat, the target control

variable involved in the mechanisms underlying the functioning of the vascular resistance BR arm – *i.e.*, vasoconstriction in the arterioles in systemic circulation – is modulated almost exclusively by the sympathetic part of the autonomic nervous system. Therefore, due to the norepinephrine kinetics and low conduction velocity in sympathetic nerves, a slower and more prolonged response in PVR is typically found (27). This means that PVR dynamics occur almost exclusively within the low and very low frequency bands (below 0.15 Hz) (3, 34, 53, 58, 60). Focusing on the cardiac chronotropic BR arm, it is also more methodologically appropriate to focus on LF oscillations where the influence of high-pressure baroreflex in SBP – RR interaction is more dominant (43). Somewhat surprisingly, in previous studies focused on the analysis of vascular resistance BR arm (probed mostly through the MSNA signal), the sequence method predominantly quantifying fast beat-to-beat changes occurring on short time scales was often employed (50, 53, 57, 62). Taking these considerations together, we limited the analysis of both BR arms to the LF band of the frequency spectrum.

Thirdly, we accounted that during the past decades a multitude of algorithms for evaluating the BR function in time (e.g., the sequence method) and frequency domains (*i.e.*, cross-spectral methods) have been proposed (11, 53, 55). It should be stressed that cardiovascular parameters often interact in closed loop – i.e. one parameter influences second one and *vice versa*. Therefore, novel methods developed specifically to assess directional (causal) interactions have been proposed; these methods should be preferred to assess interactions related to the baroreflex function (18, 49, 54), in our case referring to the causal directional interactions from SBP to RR and from SBP to PVR.

In view of the above considerations, taking into account the time scale of PVR and heart rate oscillations associated with BR function and the issue of causality, here we have applied a recently developed methodology to assess frequency domain causality, based on

partial spectral decomposition of autoregressive processes (14), to evaluate both the cardiac chronotropic and the vascular resistance arms of the baroreflex. This approach helps to quantify more objectively the amount of output power (RR or PVR) which, for a given oscillatory component (e.g., in the LF band), is directly due to the input (SBP), so that objective indexes of causal coupling (the spectral causality ratio) or gain of the reflex (the ratio between the output power and the input power for a given oscillation) can be computed. The newly applied method is more precise compared to the directed coherence and gain analysis used in previous studies (49, 54).

*Perspectives*

BR represents a complex physiological mechanism aimed at the maintenance of the arterial pressure homeostasis, exploiting different branches (42, 55, 57). The cardiac chronotropic BR is the most studied arm, which provides a valuable clinical and prognostic information in a variety of cardiovascular diseases, including myocardial infarction and cardiac failure (40). The quantification of one of the BR arms does not necessarily reflect functionality of another because each BR arm represents different and (at least partially) independent aspect of the overall baroreflex control (12, 42). The simultaneous evaluation of more than one component could give a more complex picture about the baroreflex regulation, because different baroreflex components may be affected specifically and differently during various pathological states (12).

*Study limitations*

Impedance cardiography represents a non-invasive, easy-to-use method enabling to measure CO changes on a beat-to-beat basis (61). In our study the impedance cardiograph (ICG) was able to estimate the CO on the beat-to-beat basis only in 35 – 40 percent of recordings. This was probably caused due to the errors in a detection of the characteristic

363 points or presence of artifacts (47). This limitation could be probably eliminated by proposing
364 new filtration / detection algorithms, which could improve the detection performance.

365 A methodological limitation to the causal analysis performed in this study lies in the
366 nature of the PVR measure, which – due to the impossibility to be recorded directly – has
367 been derived indirectly from MBP and CO recordings. This indirect derivation of PVR is such
368 that it is not measured independently of SBP, because SBP is partly related to MBP which is
369 one of the determinants of PVR. While this needs to be acknowledged as a potential source of
370 bias in the assessment of causality along the direction SBP→PVR, the issue is alleviated by
371 the fact that the dependence between SBP and PVR is instantaneous (i.e., it occurs with lag
372 zero), while the linear parametric model used to compute frequency domain causality is
373 dynamic (i.e., it quantifies causality according to a time-lagged concept).

374 In several subjects, the algorithm calculated zero spectral gain or spectral causality
375 values. This occurred for the spectral gain measures in 26, 3, 15, and 15 percents of subjects
376 in the SBP→RR direction (the cardiac chronotropic arm) and 8, 0, 6, and 6 percents of
377 subjects in the SBP→PVR direction (the vascular resistance arm) during supine rest, HUT,
378 supine recovery and MA respectively. The percentage of subjects with zero spectral causality
379 was 23, 3, 15, and 15 percents in the SBP→RR direction (the cardiac chronotropic arm) and
380 3,0,0, and 8 percents in the SBP→PVR direction (the vascular resistance arm) during supine
381 rest, HUT, supine recovery and MA respectively. Zero spectral causality was measured in the
382 cases where LF band spectral component of the target signals were of very low magnitude. To
383 increase the sensitivity of the method to detect non-zero gain, higher model order can be
384 employed – in any case, the gain would be very low for these subjects/phases.

385 Although the physiological control systems are inherently nonlinear (44, 45), our data
386 analysis technique assumes that in a small range of analyzed beat-to-beat fluctuations the
387 system nonlinearity does not play a significant role and a linear model is sufficient to reliably

describe the observed changes (46). In previous studies, only weak nonlinearity in the baroreflex interactions assessed from spontaneous cardiovascular parameters oscillations was demonstrated in dogs and humans (46, 56). More specifically, a dominant linear behavior in vascular arm of baroreflex (analyzed as a connection between systolic arterial pressure and sympathetic nerve activity) was found in rats (44) although several nonlinear characteristics enabled to distinguish between normo- and hypertensive rats (45). Therefore in our study linear model was employed due to its relative simplicity and results interpretability.

*Conclusion*

Considering important physiological and methodological features of baroreflex function like PVR as a target, slower time scale and causality, we have introduced a methodology for vascular baroreflex function quantification. While baroreflex involvement in both arms become more dominant during orthostatic challenge but not during mental arithmetics, gain of baroreflex interactions is relatively stable across conditions. The gender differences could indicate the dominance of vascular over cardiac chronotropic baroreflex control at rest in women requiring further study.

## Disclosures

No conflicts of interest, financial or otherwise, are declared by the authors.


## Acknowledgments

Research was supported by the grants APVV-0235-12, VEGA 1/0117/17, VEGA 1/0199/19, VEGA 1/0200/19, UK/66/2019 and project “Biomedical Center Martin” ITMS code: 26220220187, the project co-financed from EU sources. L.F. is supported in part by the Italian National PRIN 2017, PRJ-0167, “Stochastic forecasting in complex systems”, University of Palermo, Italy. R.P. is supported by the Italian PON R&I 2014-2020 AIM project no. AIM1851228-2, University of Palermo, Italy.

Author contributions: M.J., L.F. and J.K. conceptualized the study; L.F., J.K and R.P conceived and designed the analysis; J.K., B.C., N.M., R.W. and Z.T performed the investigation; J.K. and B.C. performed the data curation; J.K. prepared the original draft; M.J., L.F. and J.K edited and revised manuscript; M.J. and A.B. administrated the project. All authors have approved the final manuscript.

## *APPENDIX – Computation of Spectral Coupling and Spectral Gain*

The evaluation of spectral causality and gain is performed in this study by modelling the input time series $y_1$ (SBP) and the output time series $y_2$ (RR interval or PVR) by means of a linear bivariate autoregressive model:

$$Y(n) = \sum_{k=0}^{p} \mathbf{A}(k) Y(n-k) + W(n), \qquad \text{(A1)}$$

where $Y(n)=[y_1(n)\ y_2(n)]$ and $W(n)=[w_1(n)\ w_2(n)]^T$ are vectors containing the two time series and two noise time series (prediction errors), $\mathbf{A}(k)$ are 2×2 coefficient matrices containing the regression coefficients, and $p$ is the model order (number of lags considered in the regression).

The model in eq. (A1) is identified using a least squares method, and then the estimated model coefficients are transformed in the frequency domain (14) to derive the transfer matrix $\mathbf{H}(f)$ and the spectral matrix $\mathbf{S}(f)$:

$$\mathbf{H}(f) = \begin{bmatrix} H_{11}(f) & H_{12}(f) \\ H_{21}(f) & H_{22}(f) \end{bmatrix} \mathbf{S}(f) = \begin{bmatrix} S_{11}(f) & S_{12}(f) \\ S_{21}(f) & S_{22}(f) \end{bmatrix}, \qquad \text{(A2)}$$

which are related to each other as described in (14). The spectral matrix contains the power spectrum of the two time series, $S_{11}(f)$ and $S_{22}(f)$, as diagonal elements, and their cross-spectra, $S_{12}(f)$ and $S_{21}(f)$, as off-diagonal elements. The transfer matrix quantifies in the frequency domain the intrinsic dynamics of each time series through the diagonal elements $H_{11}(f)$ and $H_{22}(f)$, and the causal effects from one time series to the other through the off-diagonal elements $H_{12}(f)$ and $H_{21}(f)$. Exploiting the relations between the transfer and

spectral matrices (14), the power spectrum of the time series $y_2$ can be decomposed in two partial spectra

$$S_{22}(f) = S_{2|2}(f) + S_{2|1}(f) = \sigma_2^2|H_{22}(f)|^2 + \sigma_1^2|H_{21}(f)|^2, \qquad \text{(A3)}$$

where $\sigma_1^2$ and $\sigma_2^2$ are the variances of the noises $w_1$ and $w_2$ (a similar relation holds intuitively for the power of $y_1$). The partial spectra $S_{2|2}(f)$ and $S_{2|1}(f)$ describe respectively the portion of the spectrum of $y_2$ which due to its intrinsic dynamics and which is causally due to the dynamics of other the time series $y_1$.

In turn, each partial spectrum can be decomposed in spectral components related to the poles of the of the corresponding transfer function. Specifically, the spectral decomposition method (6) allows to expand the intrinsic power spectrum $S_{2|2}(f)$ and the causal power spectrum $S_{2|1}(f)$ as the sum of $q$ components:

$$S_{2|2}(f) = \sum_{k=1}^{q} S_{2|2}^{(k)}(f)\,,\; S_{2|1}(f) = \sum_{k=1}^{q} S_{2|1}^{(k)}(f). \qquad \text{(A4)}$$

The *k*-th spectral component corresponds to the *k*-th pole of the corresponding transfer function represented in the complex domain and, as such, it is associated to an oscillation of the time series with specific frequency and power content. The number $q$ of components depends on the model order $p$. Moreover, since the poles are the same for all transfer functions, the frequency of the $q$ oscillations into which the time series are decomposed is the same for the causal and intrinsic components (14). This allows to locate components on the basis of their frequency (e.g., in this study we consider those belonging to the LF band). Then, through integration over the whole frequency range we can compute the power associated to each component, $P_{2|2}^{(k)} = \int S_{2|2}^{(k)}(f)\,df$, $P_{2|1}^{(k)} = \int S_{2|1}^{(k)}(f)\,df$, and finally define the spectral coupling from $y_1$ to $y_2$ as the ratio between the causal power and the total power associated with the component in the target series

$$SC_{1\to2}(k) = \frac{P_{2|1}^{(k)}}{P_{2|1}^{(k)} + P_{2|2}^{(k)}}, \quad \text{(A5)}$$

and the spectral gain from $y_1$ to $y_2$ as the squared root of the ratio of the causal power of the component and the total power of the same component in the driving series

$$SG_{1\to2}(k) = \sqrt{\frac{P_{2|1}^{(k)}}{P_{1|1}^{(k)} + P_{1|2}^{(k)}}} \quad \text{(A6)}$$

With these definitions, the spectral coupling and gain reflect – at the frequency of any given spectral component – the fraction of the variability of the output time series that is causally due to the input series, and the portion of the variability of the output caused by the input relative to the total variability of the input time series.

The spectral causality is an adimensional measure, normalized between 0 and 1 and reflecting on the strength of the causal coupling from the input to the output time series at one specific frequency. The spectral gain is expressed in units of measurement of the output series divided by units of measurement of the input series (in this study, ms/mmHg for the cardiac chronotropic BR arm, and min/L for the vascular resistance BR arm). In this study, both measures where evaluated for the oscillatory components with frequency contained in the LF band of the spectrum.

## References


1. **Aletti F, Bassani T, Lucini D, Pagani M, and Baselli G.** Multivariate decomposition of arterial blood pressure variability for the assessment of arterial control of circulation. *IEEE transactions on bio-medical engineering* 56: 1781-1790, 2009.
2. **Aletti F, Ferrario M, Xu D, Greaves DK, Shoemaker JK, Arbeille P, Baselli G, and Hughson RL.** Short-term variability of blood pressure: effects of lower-body negative pressure and long-duration bed rest. *American journal of physiology Regulatory, integrative and comparative physiology* 303: R77-85, 2012.
3. **Aletti F, Hammond RL, Sala-Mercado JA, Chen X, O'Leary DS, Baselli G, and Mukkamala R.** Cardiac output is not a significant source of low frequency mean arterial pressure variability. *Physiological measurement* 34: 1207-1216, 2013.

4. **Barbic F, Heusser K, Marchi A, Zamuner AR, Gauger P, Tank J, Jordan J, Diedrich A, Robertson D, Dipaola F, Achenza S, Porta A, and Furlan R.** Cardiovascular parameters and neural sympathetic discharge variability before orthostatic syncope: role of sympathetic baroreflex control to the vessels. *Physiological measurement* 36: 633-641, 2015.
5. **Barbieri R, Triedman JK, and Saul JP.** Heart rate control and mechanical cardiopulmonary coupling to assess central volume: a systems analysis. *American journal of physiology Regulatory, integrative and comparative physiology* 283: R1210-1220, 2002.
6. **Baselli G, Porta A, Rimoldi O, Pagani M, and Cerutti S.** Spectral decomposition in multichannel recordings based on multivariate parametric identification. *IEEE Transactions on Biomedical Engineering* 44: 1092-1101, 1997.
7. **Borgers AJ, van den Born BJ, Alkemade A, Eeftinck Schattenkerk DW, van Lieshout JJ, Wesseling KH, Bisschop PH, and Westerhof BE.** Determinants of vascular and cardiac baroreflex sensitivity values in a random population sample. *Medical & biological engineering & computing* 52: 65-73, 2014.
8. **Camm AJ, Malik M, Bigger JT, Breithardt G, Cerutti S, Cohen RJ, Coumel P, Fallen EL, Kennedy HL, and Kleiger R.** Heart rate variability: standards of measurement, physiological interpretation and clinical use. Task Force of the European Society of Cardiology and the North American Society of Pacing and Electrophysiology. 1996.
9. **Convertino VA.** Gender differences in autonomic functions associated with blood pressure regulation. *The American journal of physiology* 275: R1909-1920, 1998.
10. **Cooke WH, Hoag JB, Crossman AA, Kuusela TA, Tahvanainen KU, and Eckberg DL.** Human responses to upright tilt: a window on central autonomic integration. *The Journal of physiology* 517 ( Pt 2): 617-628, 1999.
11. **Di Rienzo M, Parati G, Castiglioni P, Tordi R, Mancia G, and Pedotti A.** Baroreflex effectiveness index: an additional measure of baroreflex control of heart rate in daily life. *American journal of physiology Regulatory, integrative and comparative physiology* 280: R744-751, 2001.
12. **Dutoit AP, Hart EC, Charkoudian N, Wallin BG, Curry TB, and Joyner MJ.** Cardiac baroreflex sensitivity is not correlated to sympathetic baroreflex sensitivity within healthy, young humans. *Hypertension* 56: 1118-1123, 2010.
13. **Elstad M, Walloe L, Chon KH, and Toska K.** Low-frequency fluctuations in heart rate, cardiac output and mean arterial pressure in humans: what are the physiological relationships? *Journal of hypertension* 29: 1327-1336, 2011.
14. **Faes L, Krohova J, Pernice R, Busacca A, and Javorka M.** A new Frequency Domain Measure of Causality based on Partial Spectral Decomposition of Autoregressive Processes and its Application to Cardiovascular Interactions*. *2019 41st Annual International Conference of the IEEE Engineering in Medicine and Biology Society (EMBC)*, 2019, p. 4258-4261.
15. **Faes L, Mase M, Nollo G, Chon KH, and Florian JP.** Measuring postural-related changes of spontaneous baroreflex sensitivity after repeated long-duration diving: frequency domain approaches. *Autonomic neuroscience : basic & clinical* 178: 96-102, 2013.
16. **Faes L, Nollo G, and Porta A.** Information domain approach to the investigation of cardio-vascular, cardio-pulmonary, and vasculo-pulmonary causal couplings. *Frontiers in physiology* 2: 80, 2011.
17. **Faes L, Nollo G, and Porta A.** Mechanisms of causal interaction between short-term RR interval and systolic arterial pressure oscillations during orthostatic challenge. *Journal of applied physiology* 114: 1657-1667, 2013.
18. **Faes L, Nollo G, and Porta A.** Non-uniform multivariate embedding to assess the information transfer in cardiovascular and cardiorespiratory variability series. *Computers in biology and medicine* 42: 290-297, 2012.
19. **Fu Q, Shook RP, Okazaki K, Hastings JL, Shibata S, Conner CL, Palmer MD, and Levine BD.** Vasomotor sympathetic neural control is maintained during sustained upright posture in humans. *The Journal of physiology* 577: 679-687, 2006.
20. **Furlan R, Porta A, Costa F, Tank J, Baker L, Schiavi R, Robertson D, Malliani A, and Mosqueda-Garcia R.** Oscillatory patterns in sympathetic neural discharge and cardiovascular variables during orthostatic stimulus. *Circulation* 101: 886-892, 2000.

21. **Granger CWJ.** Investigating Causal Relations by Econometric Models and Cross-Spectral Methods. *Econometrica* 37: 424-438, 1969.
22. **Guyenet PG.** The sympathetic control of blood pressure. *Nature reviews Neuroscience* 7: 335-346, 2006.
23. **Hart EC, Head GA, Carter JR, Wallin BG, May CN, Hamza SM, Hall JE, Charkoudian N, and Osborn JW.** Recording sympathetic nerve activity in conscious humans and other mammals: guidelines and the road to standardization. *American journal of physiology Heart and circulatory physiology* 312: H1031-H1051, 2017.
24. **Chapleau MW.** Baroreceptor reflexes. In: *Primer on the autonomic nervous system*: Elsevier, 2012, p. 161-165.
25. **Chen X and Mukkamala R.** Selective quantification of the cardiac sympathetic and parasympathetic nervous systems by multisignal analysis of cardiorespiratory variability. *American journal of physiology Heart and circulatory physiology* 294: H362-371, 2008.
26. **Jansen JR, Wesseling KH, Settels JJ, and Schreuder JJ.** Continuous cardiac output monitoring by pulse contour during cardiac surgery. *European heart journal* 11 Suppl I: 26-32, 1990.
27. **Janssen BJ, Malpas SC, Burke SL, and Head GA.** Frequency-dependent modulation of renal blood flow by renal nerve activity in conscious rabbits. *The American journal of physiology* 273: R597-608, 1997.
28. **Javorka M, Czippelova B, Turianikova Z, Lazarova Z, Tonhajzerova I, and Faes L.** Causal analysis of short-term cardiovascular variability: state-dependent contribution of feedback and feedforward mechanisms. *Medical & biological engineering & computing* 55: 179-190, 2017.
29. **Javorka M, El-Hamad F, Czippelova B, Turianikova Z, Krohova J, Lazarova Z, and Baumert M.** Role of respiration in the cardiovascular response to orthostatic and mental stress. *American journal of physiology Regulatory, integrative and comparative physiology* 314: R761-R769, 2018.
30. **Javorka M, Krohova J, Czippelova B, Turianikova Z, Lazarova Z, Javorka K, and Faes L.** Basic cardiovascular variability signals: mutual directed interactions explored in the information domain. *Physiological measurement* 38: 877-894, 2017.
31. **Javorka M, Krohova J, Czippelova B, Turianikova Z, Lazarova Z, Wiszt R, and Faes L.** Towards understanding the complexity of cardiovascular oscillations: Insights from information theory. *Computers in biology and medicine* 98: 48-57, 2018.
32. **Jordan J and Biaggioni I.** Genetic influences on human baroreflex regulation. *Autonomic neuroscience : basic & clinical* 172: 23-25, 2012.
33. **Joyner MJ and Limberg JK.** Blood pressure regulation: every adaptation is an integration? *European journal of applied physiology* 114: 445-450, 2014.
34. **Julien C.** The enigma of Mayer waves: Facts and models. *Cardiovasc Res* 70: 12-21, 2006.
35. **Kamiya A, Hayano J, Kawada T, Michikami D, Yamamoto K, Ariumi H, Shimizu S, Uemura K, Miyamoto T, Aiba T, Sunagawa K, and Sugimachi M.** Low-frequency oscillation of sympathetic nerve activity decreases during development of tilt-induced syncope preceding sympathetic withdrawal and bradycardia. *American journal of physiology Heart and circulatory physiology* 289: H1758-1769, 2005.
36. **Kittnar O and Mlček M.** *Atlas fyziologických regulací*. Praha: Grada, 2009.
37. **Krzesinski P, Stanczyk A, Gielerak G, and Piotrowicz K.** The hemodynamic patterns in hypertensive men and women of different age. *Journal of human hypertension* 30: 177-185, 2016.
38. **Kuipers NT, Sauder CL, Carter JR, and Ray CA.** Neurovascular responses to mental stress in the supine and upright postures. *Journal of applied physiology* 104: 1129-1136, 2008.
39. **La Rovere MT, Maestri R, and Pinna GD.** Baroreflex sensitivity assessment-latest advances and strategies. *European Cardiology* 7: 89-92, 2011.
40. **La Rovere MT, Pinna GD, and Raczak G.** Baroreflex sensitivity: measurement and clinical implications. *Annals of noninvasive electrocardiology : the official journal of the International Society for Holter and Noninvasive Electrocardiology, Inc* 13: 191-207, 2008.
41. **Lucini D, Porta A, Milani O, Baselli G, and Pagani M.** Assessment of arterial and cardiopulmonary baroreflex gains from simultaneous recordings of spontaneous cardiovascular and respiratory variability. *Journal of hypertension* 18: 281-286, 2000.

42. **Marchi A, Bari V, De Maria B, Esler M, Lambert E, Baumert M, and Porta A.** Simultaneous Characterization of Sympathetic and Cardiac Arms of the Baroreflex through Sequence Techniques during Incremental Head-Up Tilt. *Frontiers in physiology* 7: 438, 2016.
43. **Mortola JP, Marghescu D, and Siegrist-Johnstone R.** Thinking about breathing: Effects on respiratory sinus arrhythmia. *Respiratory physiology & neurobiology* 223: 28-36, 2016.
44. **Moslehpour M, Kawada T, Sunagawa K, Sugimachi M, and Mukkamala R.** Nonlinear identification of the total baroreflex arc. *American journal of physiology Regulatory, integrative and comparative physiology* 309: R1479-1489, 2015.
45. **Moslehpour M, Kawada T, Sunagawa K, Sugimachi M, and Mukkamala R.** Nonlinear identification of the total baroreflex arc: chronic hypertension model. *American journal of physiology Regulatory, integrative and comparative physiology* 310: R819-827, 2016.
46. **Mukkamala R, Kim JK, Li Y, Sala-Mercado J, Hammond RL, Scislo TJ, and O'Leary DS.** Estimation of arterial and cardiopulmonary total peripheral resistance baroreflex gain values: validation by chronic arterial baroreceptor denervation. *American journal of physiology Heart and circulatory physiology* 290: H1830-1836, 2006.
47. **Naidu SMM, Pandey PC, Bagal UR, and Hardas SP.** Beat-to-beat estimation of stroke volume using impedance cardiography and artificial neural network. *Medical & biological engineering & computing* 56: 1077-1089, 2018.
48. **Nollo G, Faes L, Pellegrini B, Porta A, and Antolini R.** Synchronization index for quantifying nonlinear causal coupling between RR interval and systolic arterial pressure after myocardial infarction. *Computers in Cardiology 2000. Vol. 27 (Cat. 00CH37163)*. IEEE, 2000, p. 143-146.
49. **Nollo G, Faes L, Porta A, Antolini R, and Ravelli F.** Exploring directionality in spontaneous heart period and systolic pressure variability interactions in humans: implications in the evaluation of baroreflex gain. *American journal of physiology Heart and circulatory physiology* 288: H1777-1785, 2005.
50. **O'Leary DD, Kimmerly DS, Cechetto AD, and Shoemaker JK.** Differential effect of head-up tilt on cardiovagal and sympathetic baroreflex sensitivity in humans. *Experimental physiology* 88: 769-774, 2003.
51. **O'Leary DD, Shoemaker JK, Edwards MR, and Hughson RL.** Spontaneous beat-by-beat fluctuations of total peripheral and cerebrovascular resistance in response to tilt. *American journal of physiology Regulatory, integrative and comparative physiology* 287: R670-679, 2004.
52. **Park J, Marvar PJ, Liao P, Kankam ML, Norrholm SD, Downey RM, McCullough SA, Le NA, and Rothbaum BO.** Baroreflex dysfunction and augmented sympathetic nerve responses during mental stress in veterans with post-traumatic stress disorder. *The Journal of physiology* 595: 4893-4908, 2017.
53. **Porta A, Bari V, Maria B, Cairo B, Vaini E, Malacarne M, Pagani M, and Lucini D.** Peripheral Resistance Baroreflex During Incremental Bicycle Ergometer Exercise: Characterization and Correlation With Cardiac Baroreflex. *Frontiers in physiology* 9: 688, 2018.
54. **Porta A, Furlan R, Rimoldi O, Pagani M, Malliani A, and van de Borne P.** Quantifying the strength of the linear causal coupling in closed loop interacting cardiovascular variability signals. *Biological cybernetics* 86: 241-251, 2002.
55. **Porta A, Marchi A, Bari V, De Maria B, Esler M, Lambert E, and Baumert M.** Assessing the strength of cardiac and sympathetic baroreflex controls via transfer entropy during orthostatic challenge. *Philosophical transactions Series A, Mathematical, physical, and engineering sciences* 375, 2017.
56. **Raymundo H, Scher AM, O'Leary DS, and Sampson PD.** Cardiovascular control by arterial and cardiopulmonary baroreceptors in awake dogs with atrioventricular block. *The American journal of physiology* 257: H2048-2058, 1989.
57. **Reyes Del Paso GA, de la Coba P, Martin-Vazquez M, and Thayer JF.** Time domain measurement of the vascular and myocardial branches of the baroreflex: A study in physically active versus sedentary individuals. *Psychophysiology* 54: 1528-1540, 2017.
58. **Rosenbaum M and Race D.** Frequency-response characteristics of vascular resistance vessels. *The American journal of physiology* 215: 1397-1402, 1968.

59. **Saul JP, Berger RD, Albrecht P, Stein SP, Chen MH, and Cohen RJ.** Transfer function analysis of the circulation: unique insights into cardiovascular regulation. *The American journal of physiology* 261: H1231-1245, 1991.
60. **Saul JP, Rea RF, Eckberg DL, Berger RD, and Cohen RJ.** Heart rate and muscle sympathetic nerve variability during reflex changes of autonomic activity. *The American journal of physiology* 258: H713-721, 1990.
61. **Siedlecka J, Siedlecki P, and Bortkiewicz A.** Impedance cardiography - Old method, new opportunities. Part I. Clinical applications. *International journal of occupational medicine and environmental health* 28: 27-33, 2015.
62. **Taylor CE, Witter T, El Sayed K, Hissen SL, Johnson AW, and Macefield VG.** Relationship between spontaneous sympathetic baroreflex sensitivity and cardiac baroreflex sensitivity in healthy young individuals. *Physiological reports* 3, 2015.
63. **Vaschillo EG, Vaschillo B, Buckman JF, Pandina RJ, and Bates ME.** Measurement of vascular tone and stroke volume baroreflex gain. *Psychophysiology* 49: 193-197, 2012.
64. **Vianna LC, Fernandes IA, Martinez DG, Teixeira AL, Silva BM, Fadel PJ, and Nobrega ACL.** Water drinking enhances the gain of arterial baroreflex control of muscle sympathetic nerve activity in healthy young humans. *Experimental physiology* 103: 1318-1325, 2018.
65. **Wesseling KH, Jansen JR, Settels JJ, and Schreuder JJ.** Computation of aortic flow from pressure in humans using a nonlinear, three-element model. *Journal of applied physiology* 74: 2566-2573, 1993.
66. **Widjaja D, Montalto A, Vlemincx E, Marinazzo D, Van Huffel S, and Faes L.** Cardiorespiratory Information Dynamics during Mental Arithmetic and Sustained Attention. *PloS one* 10: e0129112, 2015.
67. **Xiajuan Z, Ding D, Yanyan H, and Zhen H.** Impedance cardiographic hemodynamic variables and hypertension in elderly Han residents. *Upsala journal of medical sciences* 118: 80-86, 2013.
68. **Xu D, Verma AK, Garg A, Bruner M, Fazel-Rezai R, Blaber AP, and Tavakolian K.** Significant role of the cardiopostural interaction in blood pressure regulation during standing. *American journal of physiology Heart and circulatory physiology* 313: H568-H577, 2017.

## Figure legends

**Fig. 1** Flowchart describing the baroreflex regulation of the blood pressure (36). Red and blue arrows illustrate the direction of changes accompanying blood pressure increase or decrease, respectively. Our study was focused on the cardiac chronotropic (left pathway) and vascular resistance (right pathway) arms.

**Fig. 2** Example of causal spectral decomposition of the interactions from SBP to RR interval and from SBP to PVR. (a-c) The time series of SBP ($y_1$, black), RR interval ($y_2$, blue) and PVR ($y_3$, red) are reported for a representative subject in the phase 1 of the protocol. (d) The power spectrum of the driver time series, SBP, is given by $\boldsymbol{S_1(f)}$ (solid line) and is decomposed, using the spectral decomposition method (14), into contributions associated to the oscillatory components of the time series; the second component $\boldsymbol{S_1^{(2)}(f)}$ evidenced in gray is the component in the LF band (central frequency ~0.11 Hz in this example). (e) The power spectrum of the first target, RR, is given by $S_2(f)$ (solid line) and is decomposed as the sum of a causal spectrum ($\boldsymbol{S_{2|1}(f)}$, black dashed) and a non-causal spectrum ($\boldsymbol{S_{2|2}(f)}$, blue dashed); (f,g) the causal and non-causal spectra are in turn decomposed into contributions associated to specific oscillations, with those in the LF band given by $\boldsymbol{S_{2|2}^{(2)}(f)}$ (non-causal part, blue shade in (f)) and $\boldsymbol{S_{2|1}^{(2)}(f)}$ (causal part, gray shade in (g)). Finally, the spectral coupling index from SBP to RR in the LF band is computed as the ratio between the power $\boldsymbol{P_{2|1}^{(2)}(LF)}$ (gray area) and the total power $\boldsymbol{P_{2|1}^{(2)}(LF) + P_{2|2}^{(2)}(LF)}$ (blue+gray areas), and the spectral gain index is computed as the squared root of the ratio between the power $\boldsymbol{P_{2|1}^{(2)}(LF)}$ (gray area in (g)) and the power $\boldsymbol{P_1^{(2)}(LF)}$ (gray area in (d)). (f-h) The same procedure applies to the computation of the spectral coupling and gain indexes from SBP to PRV. For more details on data analysis see Appendix.

**Fig. 3** Spectral causality (causal coupling) in the low frequency band measured along the direction of the interaction from SBP to RR (cardiac chronotropic baroreflex arm, upper panels) and from SBP to PVR (vascular resistance baroreflex arm, lower panels) during the four phases of the protocol (supine rest, HUT, supine recovery, MA). Distributions are plotted as individual values paired with lines and box plots reporting minimum and maximum values and (25,50,75)-th percentiles. $*$ denotes statistically significant difference between two neighboring phases of the protocol.

**Fig. 4** Distribution of the gain in the low frequency band measured along the direction of the interaction from SBP to RR (upper row) and from SBP to PVR (bottom row) during four phases of the protocol (supine rest, HUT, supine recovery, MA). The distributions are plotted as individual values paired with lines and box plots. $*$ denotes statistically significant difference between two neighboring phases of the protocol.

**Fig. 5** Box plots illustrating the gain in the low frequency band measured along the direction of the interaction from SBP to RR (upper row) and from SBP to PVR (bottom row) during the four phases of the protocol (supine rest, HUT, supine recovery, MA) separately for women (white boxes) and men (gray boxes). Box plots report minimum and maximum values (whiskers) and (25,50,75)-th percentiles (box with central line). Dots correspond to individual values. * denotes statistically significant gender differences.

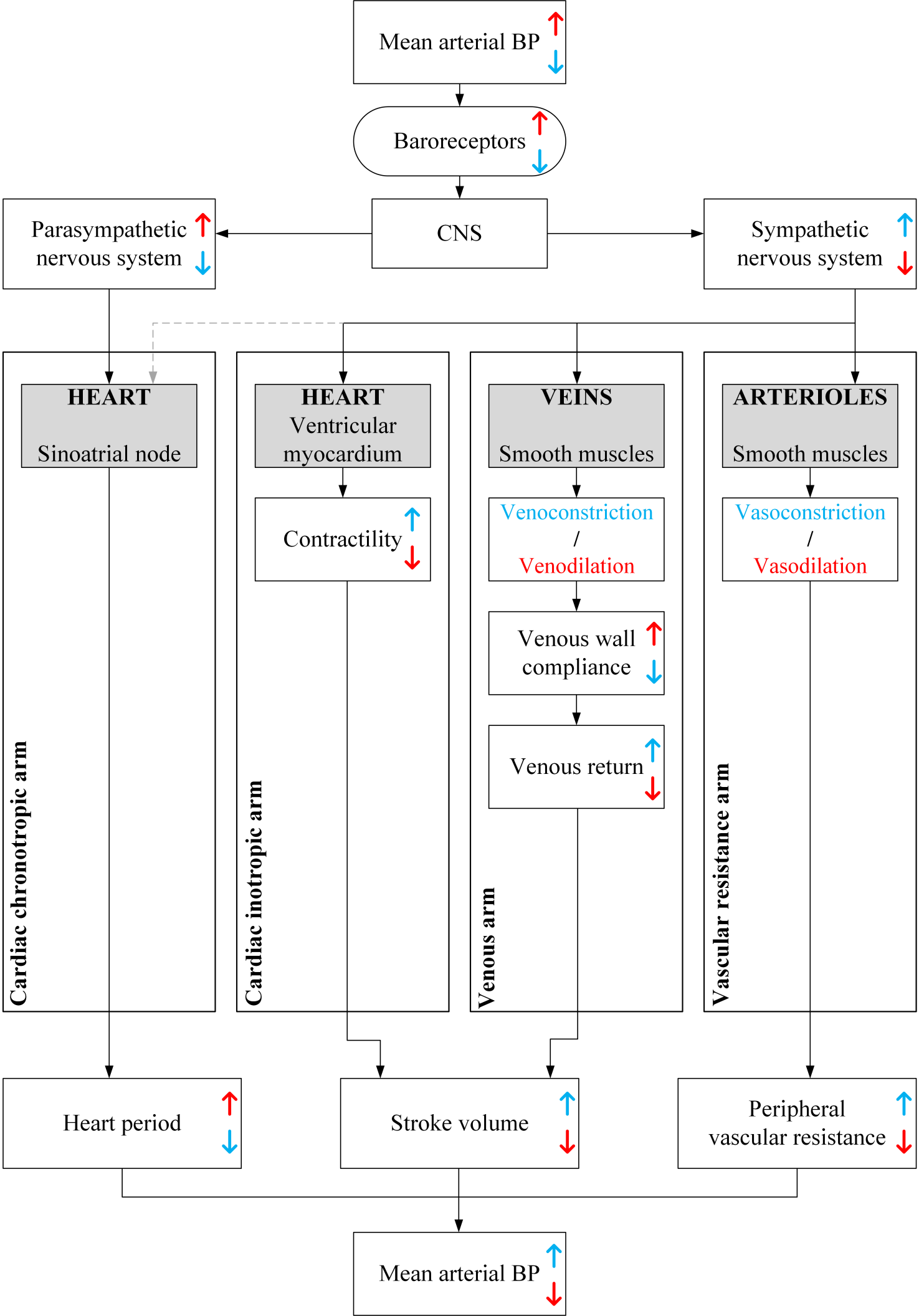
Mean arterial BP
Baroreceptors
CNS
Parasympathetic nervous system
Sympathetic nervous system
HEART
Sinoatrial node
HEART
Ventricular myocardium
VEINS
Smooth muscles
ARTERIOLES
Smooth muscles
Contractility
Venoconstriction / Venodilation
Vasoconstriction / Vasodilation
Venous wall compliance
Venous return
Cardiac chronotropic arm
Cardiac inotropic arm
Venous arm
Vascular resistance arm
Heart period
Stroke volume
Peripheral vascular resistance
Mean arterial BP

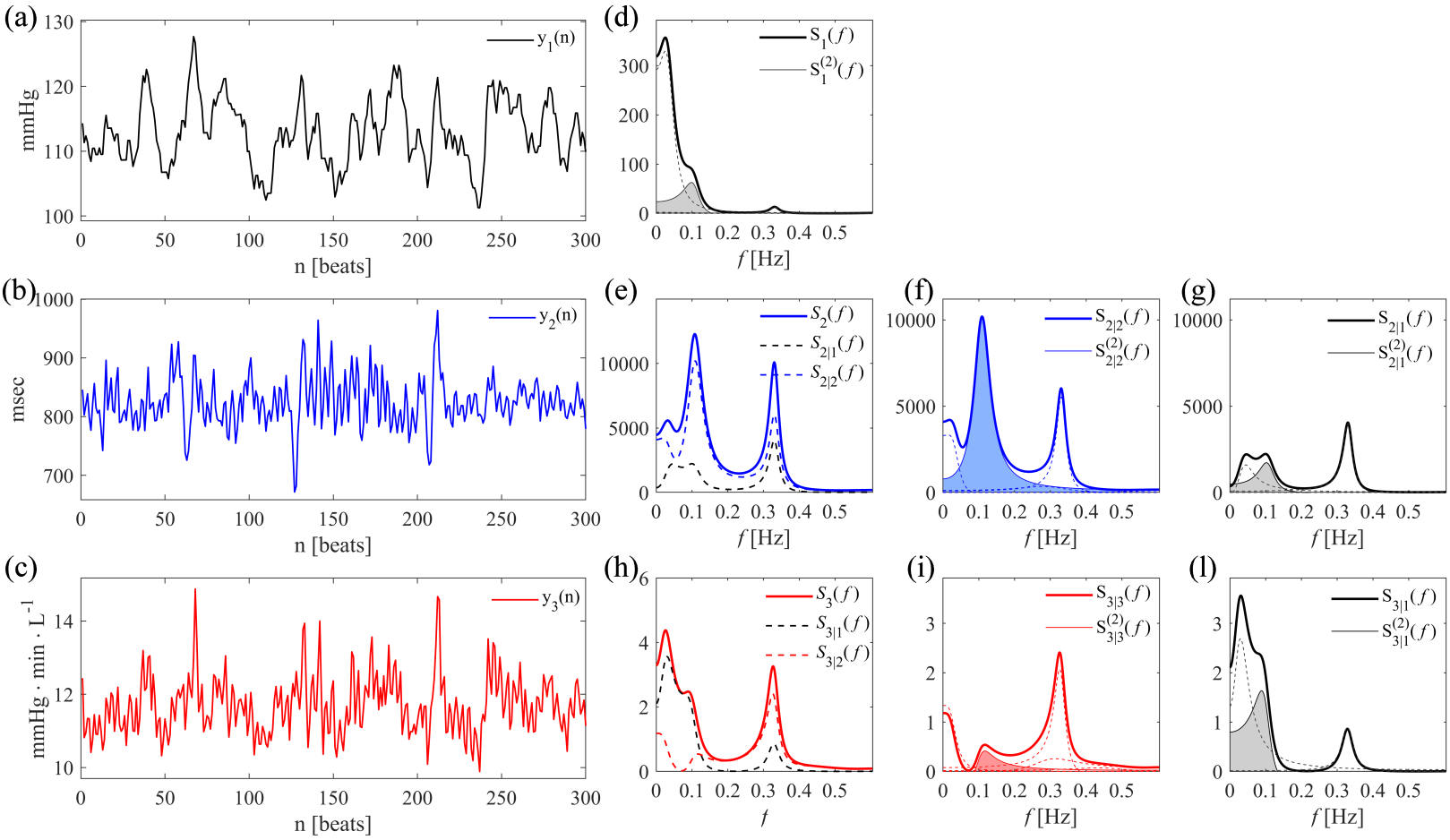
(a)
(b)
(c)
(d)
(e)
(f)
(g)
(h)
(i)
(l)
mmHg
msec
mmHg · min · L-1
n [beats]
f [Hz]
f
y1(n)
y2(n)
y3(n)
S1(f)
S1(2)(f)
S2(f)
S2|1(f)
S2|2(f)
S2|2(f)
S2|2(2)(f)
S2|1(f)
S2|1(2)(f)
S3(f)
S3|1(f)
S3|2(f)
S3|3(f)
S3|3(2)(f)
S3|1(f)
S3|1(2)(f)

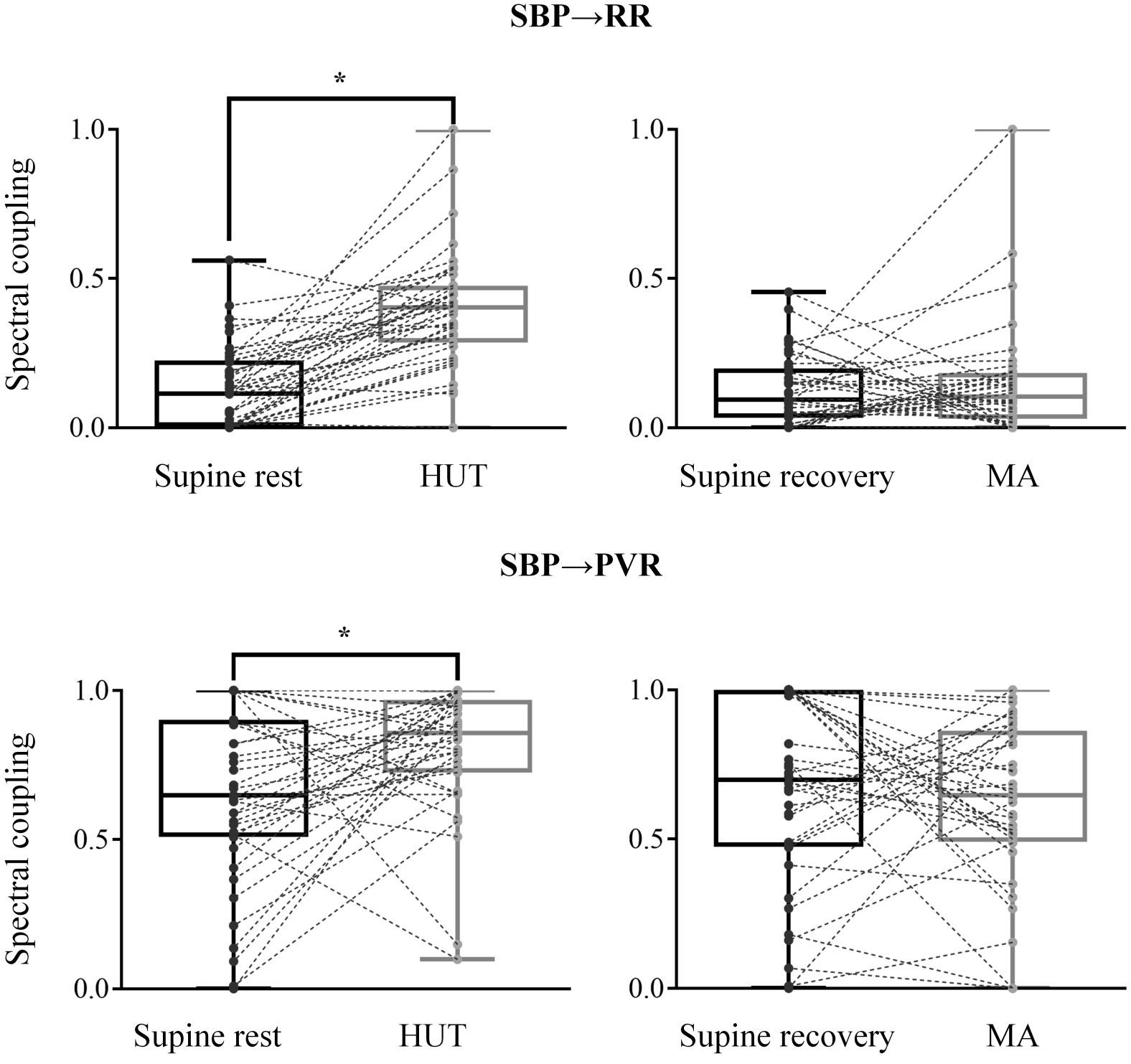
SBP→RR
*
Spectral coupling
1.0
0.5
0.0
Supine rest
HUT
Supine recovery
MA
SBP→PVR
*
Spectral coupling
1.0
0.5
0.0
Supine rest
HUT
Supine recovery
MA

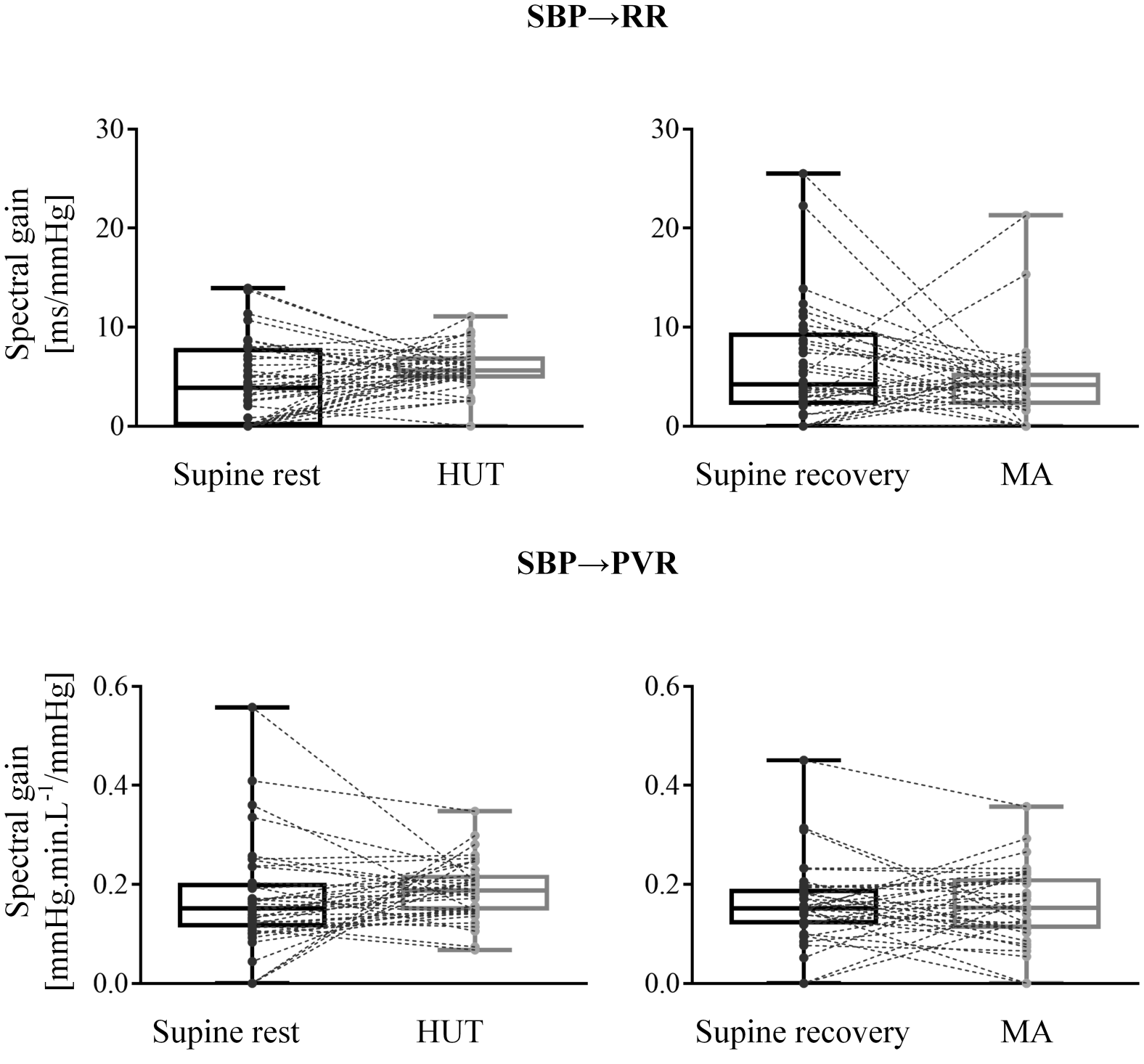
SBP→RR
Spectral gain
[ms/mmHg]
30
20
10
0
Supine rest
HUT
Supine recovery
MA
SBP→PVR
Spectral gain
[mmHg.min.L-1/mmHg]
0.6
0.4
0.2
0.0
Supine rest
HUT
Supine recovery
MA

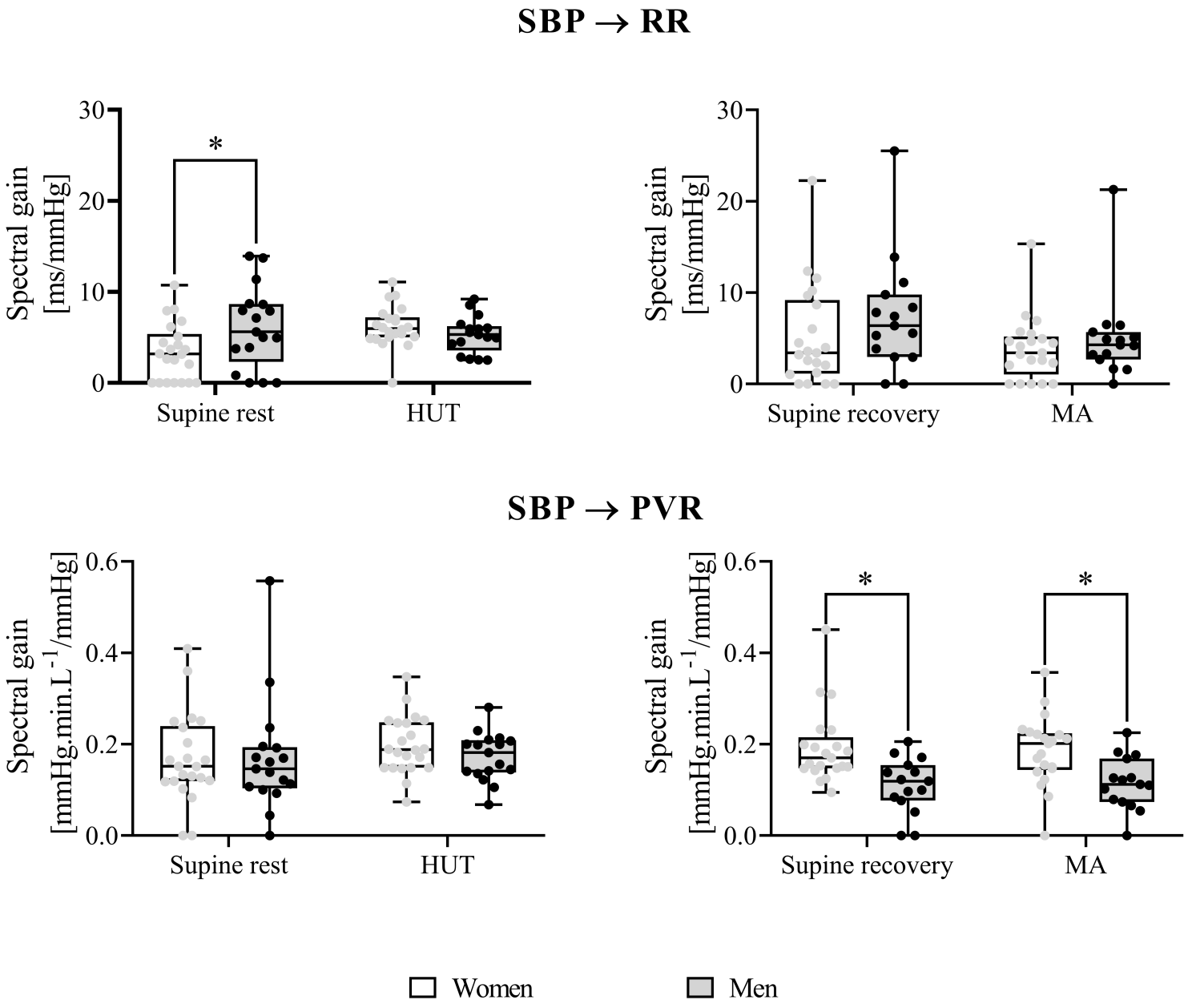
SBP → RR
Spectral gain [ms/mmHg]
30
20
10
0
*
Supine rest
HUT
Supine recovery
MA
SBP → PVR
Spectral gain [mmHg.min.L-1/mmHg]
0.6
0.4
0.2
0.0
Women
Men

**Table 1.** Basic cardiovascular and respiratory parameters averaged among all subjects for four phases of the protocol.

| | Supine rest | HUT | Supine recovery | MA |
|---|---|---|---|---|
| RR (ms) | 906.07 (91.5) | 726.41 (82.1) | 947.68 (95.7) | 804.50 (87.3) |
| SBP (mmHg) | 124.05 (8.7) | 118.14 (9.4) | 126.19 (10.7) | 136.72 (12.3) |
| MBP (mmHg) | 91.77 (5.6) | 90.05 (6.4) | 92.87 (6.7) | 102.13 (8.0) |
| DBP (mmHg) | 72.18 (5.6) | 72.90 (6.4) | 72.93 (6.5) | 80.20 (7.2) |
| CO ($L.min^{-1}$) | 6.61 (1.1) | 5.94 (0.9) | 6.65 (1.2) | 7.18 (1.4) |
| PVR ($mmHg.min.L^{-1}$) | 14.28 (2.5) | 15.55 (2.5) | 14.40 (2.5) | 14.74 (2.7) |
| Breathing frequency (Hz) | 0.34 (0.1) | 0.32 (0.1) | 0.33 (0.1) | 0.36 (0.1) |

Values are expressed as mean (SD). RR – RR interval, SBP, MBP and DBP – systolic, mean and diastolic blood pressure, respectively, CO – cardiac output, PVR – peripheral vascular resistance.